Mech Time-Depend Mater (2007) 11: 217–230
DOI 10.1007/s11043-007-9044-3

The generalized Kuhn model of linear viscoelasticity

Vassilis P. Panoskaltsis · Katerina D. Papoulia · Saurabh Bahuguna · Igor Korovajchuk

Received: 4 September 2006 / Accepted: 3 December 2007 / Published online: 15 January 2008

Abstract We propose a generalization of the Kuhn model of linear viscoelasticity. This generalization, which has four material parameters, is able to provide a near frequency independent response over a wide range of frequencies. It is useful for highly dissipative materials such as asphalt concrete. It is derived by generalizing Lubliner and Panoskaltsis's modified Kuhn model, but we also show that it is closely related to fractional derivative models. We show that the model admits a rheological approximation, that is, an approximation by classical springs and dashpots. The model and rheological representation are compared to experimental data.

Keywords Viscoelasticity · Logarithmic model · Rheological representation · Fractional derivative model · Dissipative material · Asphalt concrete

1 The generalized Kuhn model

The creep function $J(t)$ of a linear viscoelastic material is defined for $t \geq 0$ to be the strain response to a unit stress applied at $t = 0$ and held constant thereafter. In 1947, Kuhn et al. (1947) proposed the creep function

$$J(t) = B \int_0^t \frac{1 - e^{-Cx}}{x}\, dx \tag{1}$$

V.P. Panoskaltsis
Civil Engineering, Case University, Bingham Building, Cleveland, OH 44106, USA

K.D. Papoulia (✉)
Civil and Environmental Engineering, University of Waterloo, E2 Building, Waterloo, ON, N2L 3G1, Canada
e-mail: papoulia@civmail.uwaterloo.ca

S. Bahuguna
Simulia Great Lakes, 21680 Haggerty Road, Suite 103S, Northville, MI 48167, USA

I. Korovajchuk
Sest, Inc., 18000 Jefferson Park, Suite 104, Middleburg Heights, OH 44130, USA

as a model for rubber and other glassy solids. Here, B, C are material properties. This model does not support instantaneous strain (since, $J(0) = 0$) present in many real structural materials. Lubliner and Panoskaltsis (1992) modified this model by adding a constant to account for instantaneous strain response of real structural materials. They also applied a change of variables $\tau = t/(Cx)$ to the integral in (1) to obtain the modified Kuhn model. As a result of the change of variables, the creep function is written in retardation-time superposition form as

$$J(t) = A + B \int_{\lambda}^{\infty} \frac{1 - e^{-t/\tau}}{\tau} \, d\tau, \tag{2}$$

where λ in (2) stands for $1/C$ in (1). This three-parameter model can better represent concrete and other structural materials with low dissipative properties.

We propose a further generalization of this model to account for highly dissipative materials such as asphalt concrete. The generalization is the introduction a fourth parameter $\alpha \in [0, 1)$, a fractional exponent, as follows:

$$J(t) = A + B \int_{\lambda}^{\infty} \frac{1 - e^{-t/\tau}}{\tau^{1-\alpha}} \, d\tau. \tag{3}$$

The generalized Kuhn model (GKM) may also be obtained as an extension of the fractional Maxwell model as explained in Sect. 2. As with the modified Kuhn model, it is possible to develop a family of rheological approximations to the GKM, which are described in Sect. 3. These approximations are useful for finite element analysis. In Sect. 4, we show that the GKM fits experimental data for asphalt concrete closely. The modified Kuhn model is not able to fit the data as well. As discussed in Sect. 4 the data may also be fit with a series Kelvin–Voigt model, but more parameters are needed to get a good fit, and at the expense of physical meaning of the parameters.

1.1 Nomenclature

The following is a list of symbols used throughout the paper.

t	=	time, assumed to be nonnegative,
$J(t)$	=	creep function, or, equivalently strain as a function of time in response to a step-function load,
ω	=	frequency of cyclic load ($\omega > 0$),
$J^*(\omega)$	=	complex compliance, that is, Fourier transform of $J(t)$,
A, B, λ, α	=	material parameters of generalized Kuhn model,
μ, N	=	parameters of first rheological approximation to $J(t)$,
N, R	=	parameters of second rheological approximation to $J(t)$,
L	=	$\log \lambda$.

2 Comparison to fractional Maxwell model

A *fractional dashpot* is defined to be a viscoelastic object whose creep function has the form μt^{α} for some $\alpha \in (0, 1)$ and some scalar μ. Fractional dashpots are much better able to capture the properties of real materials than classical dashpots because their loss tangent is relatively insensitive to frequency. A drawback of a plain fractional dashpot is that it lacks instantaneous elasticity since the creep function is 0 at $t = 0$. This leads to consideration of

the *fractional Maxwell model* (FMM), which consists of a classical spring in series with a fractional dashpot. Its creep compliance is therefore $J(t) = J_0 + \mu t^\alpha$. As shown in Papoulia et al. (2008), this creep compliance may be rewritten as

$$J(t) = J_0 + \frac{\alpha\mu}{\Gamma(1-\alpha)} \int_0^\infty \frac{1 - e^{t/\tau}}{\tau^{1-\alpha}}\, d\tau. \tag{4}$$

Comparison of (4) to (3) shows that the FMM is a special case of the GKM obtained by taking $\lambda = 0$. Furthermore, the monotone convergence theorem (Royden 1988) implies that for any $t > 0$, $J_\lambda(t) \to J_0(t)$ as $\lambda \to 0$, where $J_\lambda(t)$ is notation for the GKM creep function in which the dependence on parameter λ is explicitly indicated. This shows that the GKM may be described as a generalization of the FMM as well as a generalization of the modified Kuhn model.

3 Rheological representation of the GKM

A difficulty with the GKM is that its representation via the creep function (3) is not easily incorporated into finite element analysis. Viscoelastic models composed of springs and dashpots, i.e., rheological models, are easily incorporated into computation because they can be described via a system of ordinary differential equations relating state variables and external stress and strain. To bridge this gap, we develop a family of rheological models whose viscoelastic behavior converges to that of the GKM. Our technique is to approximate the integral in (3) by a quadrature rule. We refer to the resulting network as a *rheological representation* of the GKM. We propose two such representations in this section. Both have the form of a series composed of N classical Kelvin–Voigt units and one spring. These representations were proposed for the FMM in Papoulia et al. (2008).

The first technique is based on a piecewise-constant quadrature rule and is based directly on a technique in Lubliner and Panoskaltsis (1992). The approximation has two parameters, N, μ such that $\mu > \lambda$. Parameter N is the number of Kelvin–Voigt units in the representation while parameter μ controls the range of frequencies for which the approximation is accurate. Let $r = (\mu/\lambda)^{1/N}$. Let $\tau_0, \ldots, \tau_N$ be defined according to the formula $\tau_m = \lambda^{(N-m)/N} \mu^{m/N}$. With this definition, the following properties hold: $\tau_0 = \lambda$, $\tau_N = \mu$, and for each intermediate m, $\tau_m = r\tau_{m-1}$, i.e., the τ_m's are geometrically spaced with ratio r. Define

$$J_{\mu,N}(t) = A + B \ln r \sum_{m=0}^{N-1} \xi_m^\alpha \left(1 - e^{-t/\tau_m}\right). \tag{5}$$

Observe that $J_{\mu,N}(t)$ is the creep function of N Kelvin–Voigt units in series.

A second technique uses midpoint quadrature as in Papoulia et al. (2008) and is therefore expected to be more accurate (since midpoint quadrature is higher order than piecewise constant approximation). Let $R > 0$ be a parameter such that $e^R > \lambda$. More details about R will be provided below. Break up (3) into three terms:

$$J(t) = A + J^{(\mathrm{i})}(t) + J^{(\mathrm{ii})}(t)$$

where

$$J^{(\mathrm{i})}(t) = B \int_\lambda^{e^R} \frac{1 - e^{-t/\tau}}{\tau^{1-\alpha}}\, d\tau \tag{6}$$

and

$$J^{(\mathrm{ii})}(t) = B\int_{e^R}^{\infty} \frac{1-e^{-t/\tau}}{\tau^{1-\alpha}}\,d\tau. \tag{7}$$

Perform a change of variables on (6) given by $\tau = e^{\theta}$ to obtain

$$J^{(\mathrm{i})}(t) = B\int_{L}^{R} (1-\exp(-t/e^{\theta}))e^{\alpha\theta}\,d\theta,$$

where $L = \ln\lambda$. Let N be the number Kelvin–Voigt units in the rheological approximation, and assume now that R depends on N in such a way that as $N\to\infty$, $R\to\infty$ while $R/N\to 0$, e.g., $R = LN^{1/2}$. To approximate the preceding formula for $J^{(\mathrm{i})}(t)$, subdivide $[L, R]$ into $N-1$ equal subintervals $[L, L+(R-L)/(N-1)], \ldots, [L+(N-2)(R-L)/(N-1), R]$. Use a compound midpoint quadrature rule based on these subintervals:

$$J^{(\mathrm{i})}_{N,R}(t) = B\sum_{m=1}^{N-1}(1-\exp(-t/e^{x_m}))e^{\alpha x_m}(R-L)/(N-1)$$

where x_m is the midpoint of the mth interval, i.e., $x_m = L+(m-1/2)(R-L)/(N-1)$.

For $J^{(\mathrm{ii})}(t)$, we develop an approximation in terms of a single Kelvin–Voigt unit by transforming this integral into the frequency domain, carrying out an approximation in that domain under the assumption that $\omega \gg e^{-R}$ (valid in the limit since $R\to\infty$ as $N\to\infty$), and then transforming back to the time domain. In particular, the Fourier transform of (7) yields

$$J^{(\mathrm{ii})*}(\omega) = B\int_{e^R}^{\infty} \frac{d\tau}{(1+i\omega\tau)\tau^{1-\alpha}}.$$

Since we assume $\omega \gg e^{-R}$, the approximation $1+i\omega\tau \approx i\omega\tau$ is valid, in which case the integral can be evaluated in closed form:

$$\begin{aligned} J^{(\mathrm{ii})*}(\omega) &\approx B\int_{e^R}^{\infty} \frac{d\tau}{(i\omega\tau)\tau^{1-\alpha}} \\ &= \frac{B}{i\omega e^{(1-\alpha)R}(1-\alpha)} \\ &= \frac{Be^{\alpha R}}{i\omega e^{R}(1-\alpha)} \\ &\approx \frac{Be^{\alpha R}}{(1+i\omega e^{R})(1-\alpha)}. \end{aligned}$$

The quantity on the last line is seen to be the frequency domain representation of a Kelvin–Voigt unit. Transforming back to the time domain yields the corresponding creep function: $J^{(\mathrm{ii})}(t) \approx J^{(\mathrm{ii})}_R(t)$ where

$$J^{(\mathrm{ii})}_R(t) = Be^{\alpha R}(1-\exp(t/e^{R}))/(1-\alpha).$$

Therefore, the complete rheological approximation to (3) is given by

$$J_{N,R}(t) = A + J^{(\mathrm{i})}(t) + J^{(\mathrm{ii})}(t)$$

$$\begin{aligned}
&\approx A + J^{(\mathrm{i})}_{N,R}(t) + J^{(\mathrm{ii})}_{R}(t) \\
&= A + B\sum_{m=1}^{N-1}(1-\exp(-t/e^{x_m}))e^{\alpha x_m}(R-L)/(N-1) \\
&\quad + Be^{\alpha R}(1-\exp(t/e^{R}))/(1-\alpha). \qquad (8)
\end{aligned}$$

A very slight modification to Theorem 1 of Papoulia et al. (2008) shows that for a fixed t, $J_{\mu,N}(t) \to J(t)$ as $N \to \infty$ and $\mu \to \infty$, provided that $(\mu/\lambda)^{1/N} \to 1$. (Here, $J_{\mu,N}$ refers to the first rheological approximation scheme.) For example, one could select $\mu = \lambda e^{\sqrt{N}}$.

In this work, we will show instead that $J^*_{N,R}(\omega) \to J^*(\omega)$ for any $\omega \to 0$, as $N \to \infty$ and $R \to \infty$ provided that $R/N \to 0$ (e.g., $R = L\sqrt{N}$). Here, $J^*_{N,R}$ refers to the frequency-domain transformation of the second approximation scheme. Note that a convergence proof for a fixed t as in the previous paragraph does not imply convergence of the Fourier transform for a fixed ω (unless the convergence argument additionally establishes uniformity of the limits). Therefore, the theorem that follows is not a consequence of results from Papoulia et al. (2008) although the proof technique is similar.

Theorem 1 *Consider a specification of the parameters λ, α, A, B in the generalized Kuhn model (3). Let $L = \ln\lambda$. Let N be a positive integer parameter, and let $R > L$ be a scalar depending on N such that $R \to \infty$ and $R/N \to 0$ as $N \to \infty$ (e.g., $R = LN^{1/2}$). Then for any $\omega > 0$, $J^*_{N,R}(\omega) \to J^*(\omega)$ as $N \to \infty$.*

Proof It follows from (3) and well-known theory of Fourier transforms (see, e.g., Golden and Graham 1988) that

$$J^*(\omega) = A + B\int_{\lambda}^{\infty} \frac{d\tau}{\tau^{1-\alpha}(1+i\omega\tau)}. \qquad (9)$$

On the other hand, by (8),

$$J^*_{N,R}(\omega) = A + B\left(\sum_{m=1}^{N-1} \frac{y_m^{\alpha}\delta}{1+i\omega y_m} + \frac{e^{\alpha R}/(1-\alpha)}{1+i\omega e^{R}}\right), \qquad (10)$$

where $y_m = \exp(x_m)$ and $\delta = (R-L)/(N-1)$. Let us explicitly denote the dependence of these parameters on N by writing y_m^N, R^N and δ^N. Partition the interval $[\lambda, \infty)$ into N subintervals $I_1^N = [\lambda, \lambda e^{\delta^N})$, $I_2^N = [\lambda e^{\delta^N}, \lambda e^{2\delta^N})$, $\ldots, I_{N-1}^N = [\lambda e^{(N-2)\delta^N}, \lambda e^{(N-1)\delta^N})$, $I_{\infty}^N = [\lambda e^{(N-1)\delta^N}, \infty)$. Recall that x_m is the midpoint of the interval $[L + (m-1)\delta^N, L + m\delta^N]$ for $m = 1, \ldots, N-1$. This means that y_m^N lies in the interval $[e^L e^{(m-1)\delta^N}, e^L e^{m\delta^N})$, which is the same as I_m^N since $\lambda = e^L$.

Notice also that the right endpoint $\lambda e^{(N-1)\delta^N}$ of I_{N-1}^N, which is also the left endpoint of I_{∞}^N, simplifies to e^R since $\delta^N = (R^N - L)/(N-1)$ and $e^L = \lambda$.

Given some arbitrary $\tau \in [\lambda, \infty)$, let $m(N, \tau)$ be the value of m such that τ lies in I_m^N. Note that for N sufficiently large, $m < \infty$ since the right endpoint of I_{N-1}^N tends to ∞ as $N \to \infty$. This is because the right endpoint is equal to e^{R^N}, and we have assumed that $R^N \to \infty$ as $N \to \infty$. Thus, for N sufficiently large, $m(N, \tau) < \infty$.

Consider only those values of N sufficiently large so that $m(N, \tau) < \infty$, and define $y(N, \tau)$ to be $y^N_{m(N,\tau)}$. We claim that $y(N, \tau) \to \tau$ as $N \to \infty$. This is because $y(N, \tau)$ and

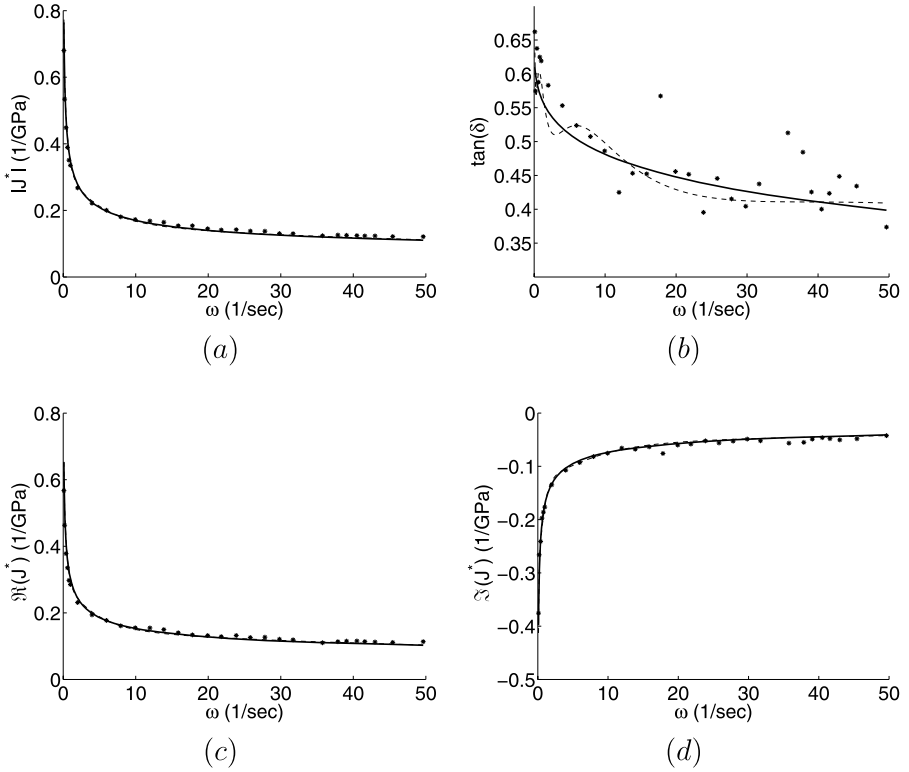

Fig. 1 The *solid curve* shows the best fit of a GKM to Dietrich's asphalt data using the procedure described in the text. Since the data being fit, $J^*(\omega)$ is complex, the quality of the fit is depicted via four real quantities: (**a**) $|J^*|$; (**b**) $\tan(\delta)$; (**c**) Real(J^*); and (**d**) Imag(J^*). In each plot, the *asterisks* are the data and the *solid line* is the GKM. In addition the rheological representation given by (10) is shown as a *dashed line* using parameters $N = 15$, $R = 4$

y_m^N (where, here, m is shorthand for $m(N,\tau)$) both lie in the same subinterval, namely I_m^N, but the width of this subinterval, which is $\lambda(e^{m\delta^N} - e^{(m-1)\delta^N})$, i.e., $\lambda e^{(m-1)\delta^N}(e^{\delta^N} - 1)$, is bounded above by $\tau(e^{\delta^N} - 1)$, and $e^{\delta^N} - 1 \to 0$ as $N \to \infty$ since $\delta \to 0$ (by the assumption that $R^N/N \to 0$ as $N \to \infty$).

Therefore, $y(N,\tau) \to \tau$. Now, for a fixed $\omega > 0$ and $N \geq 1$, consider the piecewise constant function $f_{\omega,N} : \mathbf{R} \to \mathbf{R}$ given by

$$f_{\omega,N}(\tau) = \begin{cases} \dfrac{y_m^\alpha \delta}{(1 + i\omega y_m)\lambda e^{(m-1)\delta}(e^\delta - 1)} & \text{for } \tau \in I_m,\ m = 1, \ldots, N-1, \\ 0 & \text{for } \tau \notin [\lambda, e^R), \end{cases} \tag{11}$$

where now we have written again y_m, δ, etc., for y_m^N, δ^N, etc. Observe that

$$\int_\lambda^\infty f_{\omega,N}(\tau)\, d\tau = \sum_{m=1}^{N-1} \frac{y_m^\alpha \delta}{1 + i\omega y_m}$$

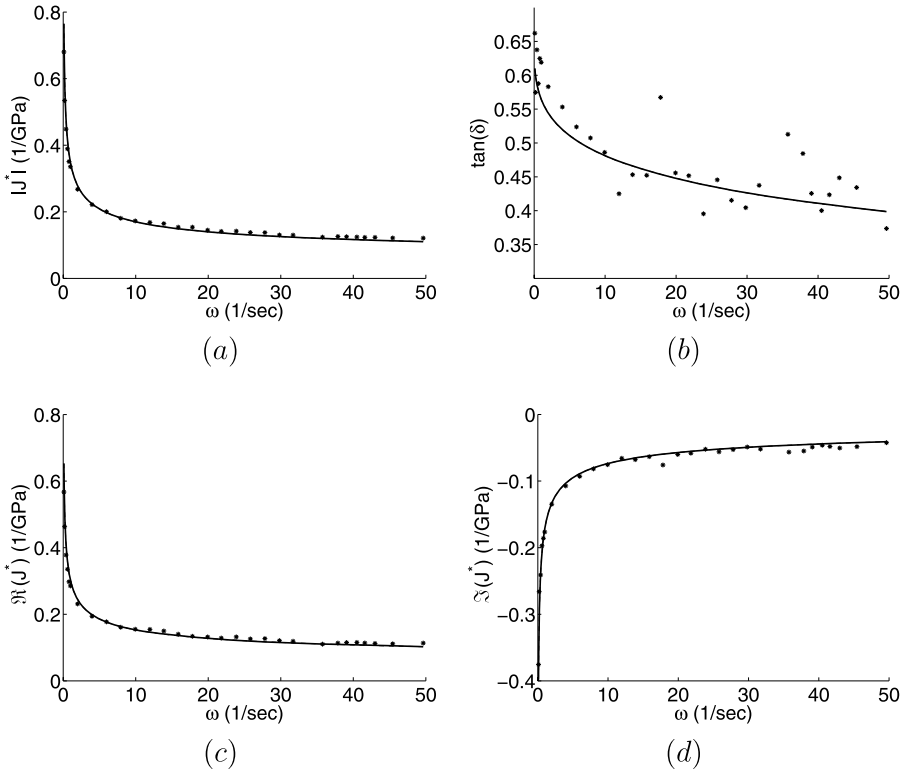

Fig. 2 This figure is identical to Fig. 1 except the rheological representation (*dashed line*, which is mostly hidden by the *solid line*) is now based on $N = 30$, $R = 6$ and hence is much closer to the GKM (*solid line*)

because the left-hand side can be written as $\int_{I_1} + \int_{I_2} + \cdots$, a sum of integrals of constant functions, and the length of interval I_m which is a factor in the mth such term, is exactly cancelled out by the factor $\lambda e^{(m-1)\delta}(e^{\delta} - 1)$ appearing in the denominator of (11). Note that the right-hand side of the previous equation is the second term (except for the scalar B) of (10).

Next, we claim that for a fixed ω and τ, $f_{\omega,N}(\tau) \to f_{\omega}(\tau)$ as $N \to \infty$, where $f_{\omega}(\tau)$ is the integrand of (9), i.e.,

$$f_{\omega}(\tau) = \frac{1}{\tau^{1-\alpha}(1 + i\omega\tau)}.$$

To show this, observe that $\delta \to 0$ as $N \to \infty$, hence $\delta/(e^{\delta} - 1) \to 1$. As argued above, $y_m \to \tau$. Since y_m and τ both lie in $[\lambda e^{(m-1)\delta}, \lambda e^{(m)\delta})$, an interval whose width is tending to zero, $\lambda e^{(m-1)\delta} \to \tau$ as $N \to \infty$. Thus, the limiting value of $f_{\omega,N}(\tau)$ is $\tau^{\alpha}/((1 + i\omega\tau)\tau)$, which is $f_{\omega}(\tau)$.

Next, consider only those values of N sufficiently large so that $\delta \leq 1$. Note that $y_m, \tau \in I_m$, and the endpoints of I_m differ by a multiplicative factor e^{δ}, which is at most e by assumption, we can claim that $\tau/e \leq y_m \leq e\tau$ and $\lambda e^{(m-1)\delta} \geq \tau/e$. Also, $\delta/(e^{\delta} - 1) \leq 1$ for all $\delta > 0$. Finally, $|1 - i\omega y_m| \geq \omega y_m$ since the imaginary part of a complex number is bounded

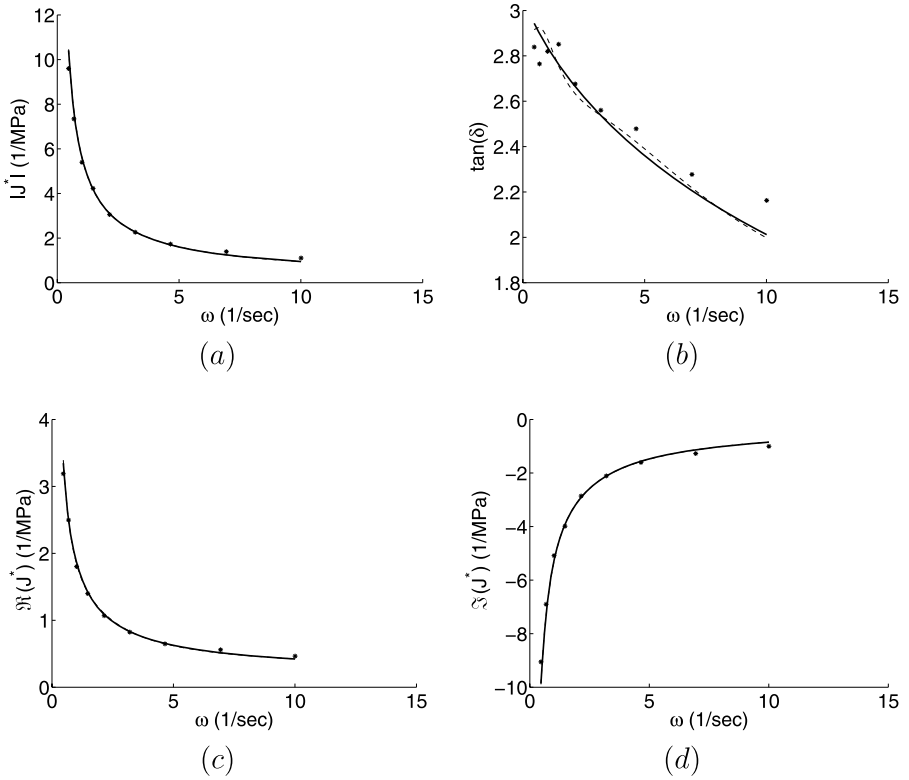

Fig. 3 This figure is analogous to Fig. 1; the data in this figure is from Cerni, and the rheological representation uses $N = 15$, $R = 7$

by its modulus. Therefore, for $\tau \in [\lambda, e^R)$,

$$\begin{aligned} |f_{\omega,N}(\tau)| &= \frac{y_m^\alpha \delta}{|1 + i\omega y_m| \cdot \lambda e^{(m-1)\delta}(e^\delta - 1)} \\ &\leq \frac{(e\tau)^\alpha}{\omega(\tau/e)(\tau/e)} \\ &= e^{\alpha+2}\tau^{\alpha-2}/\omega. \end{aligned}$$

Define $g(\tau)$ to be the right-hand side of the preceding inequality, that is, $e^{\alpha+2}\tau^{\alpha-2}/\omega$. Since $0 < \alpha < 1$, $g(\tau)$ is integrable on the interval $[\lambda, \infty)$ for any $\lambda > 0$. Since $f_{\omega,N} \to f_\omega$ pointwise and since $|f_{\omega,N}|$ is bounded by an integrable function for all N sufficiently large, the Lebesgue convergence theorem implies that

$$\int_\lambda^\infty f_{\omega,N}(\tau)\, d\tau \to \int_\lambda^\infty f_\omega(\tau)\, d\tau$$

as $N \to \infty$. This proves the second term of (10) converges to the corresponding term of (9). The third term of (10) tends to 0 as $N \to \infty$ since $R^N \to \infty$ as $N \to \infty$. This proves the theorem. □

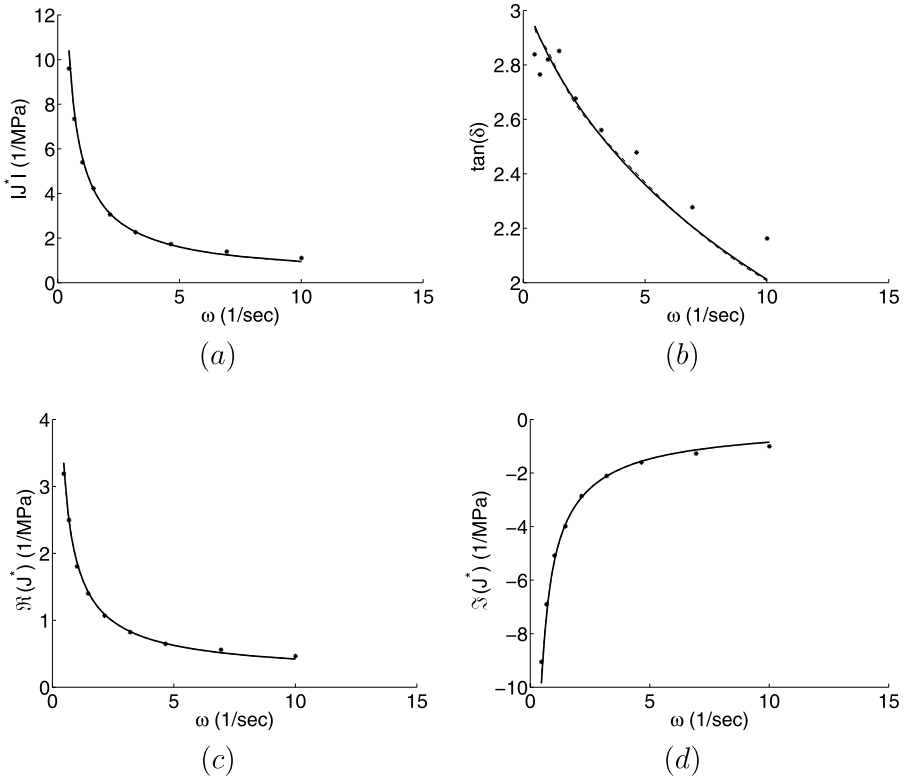

Fig. 4 This figure is identical to Fig. 3 except the rheological representation uses $N = 20$, $R = 10$

4 Asphalt experiments

In this section, we fit two sets of asphalt creep data with the generalized Kuhn model. In both cases, the data consists of ordered pairs of the form (ω_i, J_i^*), $i = 1, \ldots, n$, measured in the laboratory.

Our data-fitting procedure is as follows. We loop over a list of 60 exponentially spaced candidate values for λ. These candidate values are generated geometrically spaced in the interval $[10^{-11}, 10^2]$. This range is chosen because parameter λ has the units of time, and the relevant range of timescales for a given data set are no larger than 10^2.

Nested with the λ loop, we also loop over 60 values of α spaced evenly in $[0, 1)$. Once λ and α are fixed, it remains to select A and B. Observe that (3) is linear in A and B, so this amounts to solving a linear least-squares problem. The fitting is done on the Fourier transform given by (9). Computing the coefficients of the least-squares problem requires evaluation of the integral in (9); this is done numerically with Matlab's quad function after a change of variables given by $\tau = (\sigma/(1-\sigma))^{1/(1-\alpha)}$, which makes the interval of integration finite and also makes the integrand nonsingular.

We solve the following weighted version of the linear least squares problem

$$\min_{A,B} \left[\sum_{i=1}^{n} \left(\frac{\Re J^*(\omega_i)}{\Re J_i^*} - 1 \right)^2 + \sum_{i=1}^{n} \left(\frac{\Re J^*(\omega_i)}{\Re J_i^*} - \frac{\Im J^*(\omega_i)}{\Im J_i^*} \right)^2 \right].$$

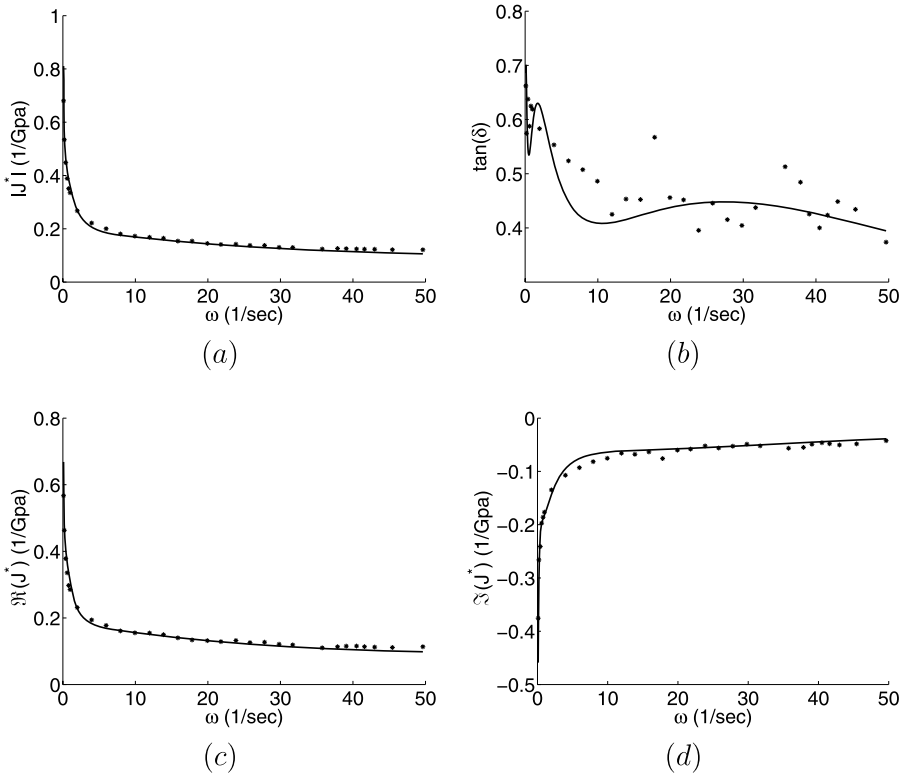

Fig. 5 This figure shows the best fit to the Dietrich data by a 3-unit SKVM model using the procedure described in the text. The four plots are the four representations of the complex fit used in the previous figures

In this expression, $J^*(\omega_i)$ denotes (3) evaluated at ω_i, in which α and λ are fixed while A and B are the scalars to be optimized, and J_i^* denotes the experimental data corresponding to ω_i. The first summation expresses the objective that the real part of $J^*(\omega)$ should be close to the real part of J_i^*. This way of writing the term (as opposed to the more obvious formulation $(\Re J^*(\omega_i) - \Re J_i^*)^2$) ensures that the experimental values with a large value of $\Re J_i^*$ do not dominate those with small values. The second term in the summation expresses the objective that the loss tangent of $J^*(\omega_i)$ should be close to the experimental loss tangent. (The loss tangents are obtained by cross-multiplying the two quotients in second term; the more obvious way to express the goodness of the loss-tangent fit, namely, $((\Im J_i^*)/(\Re J_i^*) - (\Im J^*(\omega_i))/(\Re J^*(\omega_i)))^2$, is nonlinear in A and B.) Thus, our fitting procedure involves solving 3600 linear least squares problems and keeping the best overall solution, that is, the solution with the smallest residual. It was checked that 60 candidate values for λ and 60 for α were adequate by trying refinements of both numbers and noting that a significantly better fit was not obtained.

Figure 1 shows Dietrich et al.'s (1998) asphalt data (asphalt D100 with 15% of rubber flower) plotted against the best fitting GKM. The optimal parameters found using the search procedure described above are $A = .03693/\text{GPa}$, $B = .09143/(\text{GPa} \cdot \text{s}^\alpha)$, $\lambda = 0$ s, $\alpha = .36667$. As can be seen from the figure, the fit to the data seems quite good. This figure also shows the series Kelvin–Voigt rheological representation of this GKM defined by (10) with $N = 15$, $R = 4$. The rheological representation is close to the true GKM (indeed, the

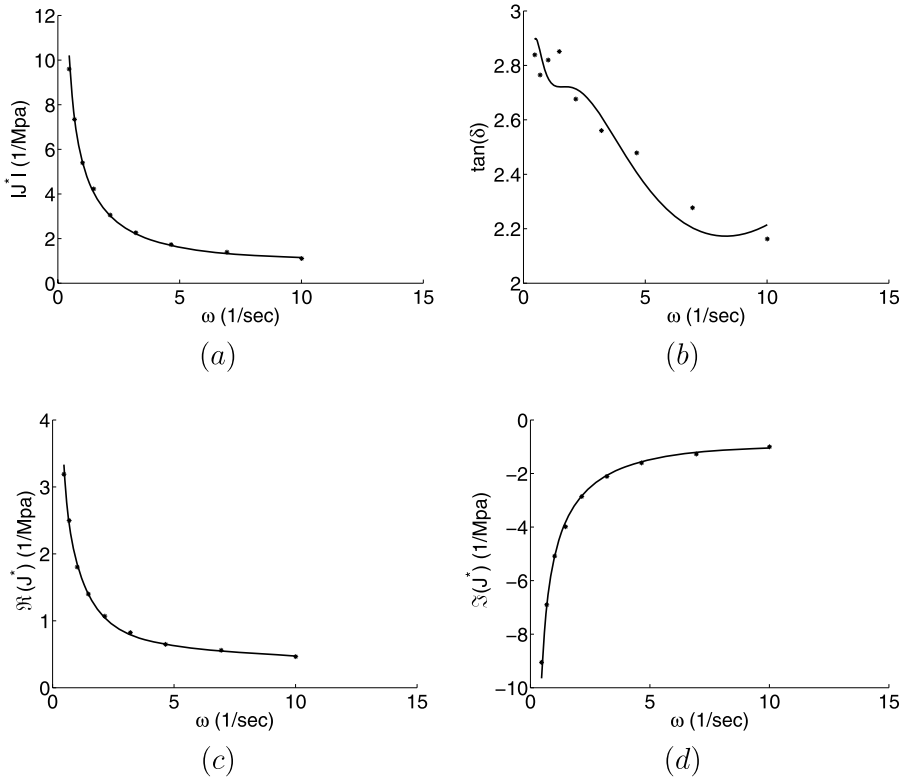

Fig. 6 This figure shows the best fit to the Cerni data by a 3-unit SKVM model using the procedure described in the text. The four plots are the four representations of the complex fit used in the previous figures

difference is not much larger than the difference between the GKM and true data). A more accurate rheological representation is shown in Fig. 2.

Figure 3 shows Cerni's asphalt data plotted against the best fitting GKM. Cerni (2001) conducted several experiments; the experiment depicted here is for modified bitumen SBS-R using 80/100 bitumen as base and tested at 35 °C. The optimal parameters for this fit are $A = 0.1459/\text{MPa}$, $B = 1.0529/(\text{GPa}\cdot \text{s}^{\alpha})$, $\lambda = 2.0 \cdot 10^{-8}$ s, $\alpha = 0.8$. Again, the plot shows a fairly good fit. This figure also shows a rheological representation of this GKM with $N = 15$, $R = 7$, and a more accurate rheological representation is shown in Fig. 4.

In order to assess the quality of these fits, it is helpful to fit other models to the same data. Recall that the rheological representation used to approximate the GKM is a series Kelvin–Voigt model (SKVM). Therefore, it is natural to ask whether a SKVM can be fit directly to the data. We attempted to fit a 3-unit SKVM directly to the data. In frequency space, the creep function for an N-unit SKVM is given by

$$J^*(\omega) = j_0 + \sum_{i=1}^{N} \frac{j_i}{1 + i\omega\tau_i}.$$

The fitting procedure was as follows. Observe from the preceding equation that once $\tau_1, \ldots, \tau_N$ are specified, fitting the data is a linear least-squares problem for $j_0 \ldots, j_N$.

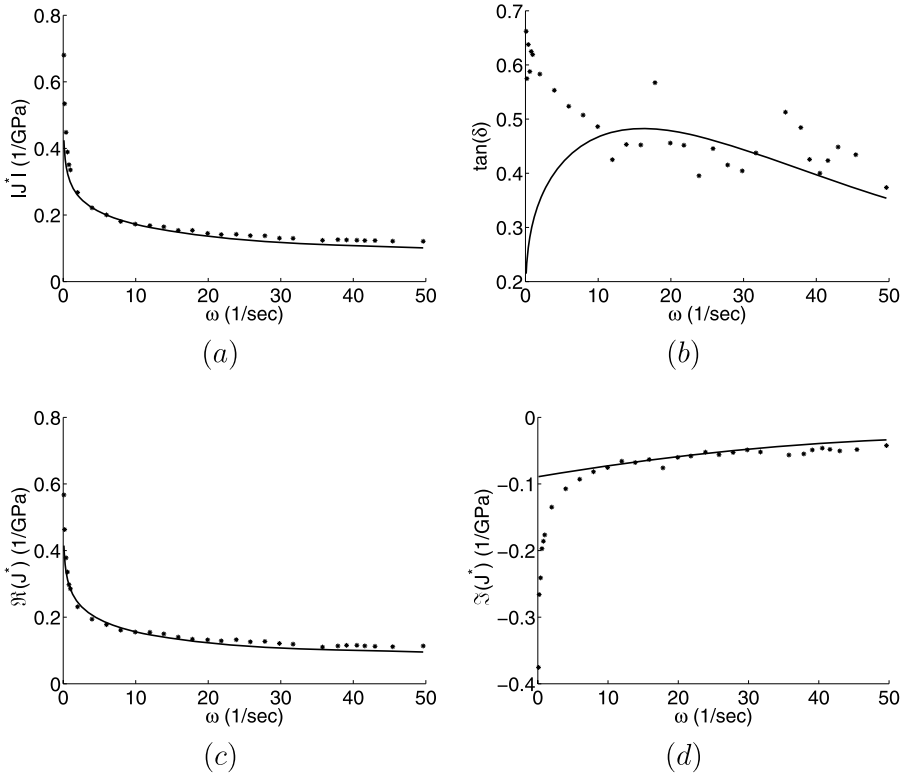

Fig. 7 This figure shows the best fit to the Dietrich data by a modified Kuhn model (MKM) using the procedure described in the text. The four plots are the four representations of the complex fit used in the previous figures

Therefore, our fitting procedure makes a predefined list of 50 exponentially spaced possible values of τ_i and tries all $\binom{50}{3}$ combinations. For each combination, a linear least-squares problem is solved to obtain the j_i's. The results of this process for this data are presented in Figs. 5 and 6. It can be observed that these fits are quite good—comparable to the quality of the GKM fit. On the other hand, a disadvantage of this model is that there is no obvious physical interpretation of the seven parameters that describe the model. A second disadvantage is that the model is prone to overfitting. Indeed, it is observed from the two figures that there is oscillation in the fitting of $\tan\delta$ that appears to be caused by noise in the data.

A final point to make about fitting an SKVM model is that there is no guarantee that the $N+1$ parameters $j_0, \ldots, j_N$ emerging from our procedure will be positive (since we used classical rather than nonnegative least-squares fitting, the latter being a much more expensive computation). Indeed, it turned out that the optimal j_0 parameter found for the Dietrich data was negative, which is physically impossible. Therefore, a more careful SKVM fitting algorithm would need to impose nonnegative constraints on the parameters. Since our usage of SKVM is merely to compare the results to GKM, and since nonnegativity constraints would necessarily decrease the quality of the SKVM fit (since the space of feasible parameter values is diminished), we did not attempt a fit based on nonnegative least squares.

A final kind of model to try for this data is the modified Kuhn model (MKM) of Lubliner and Panoskaltsis, since the GKM has been introduced in this paper to improve on MKM in

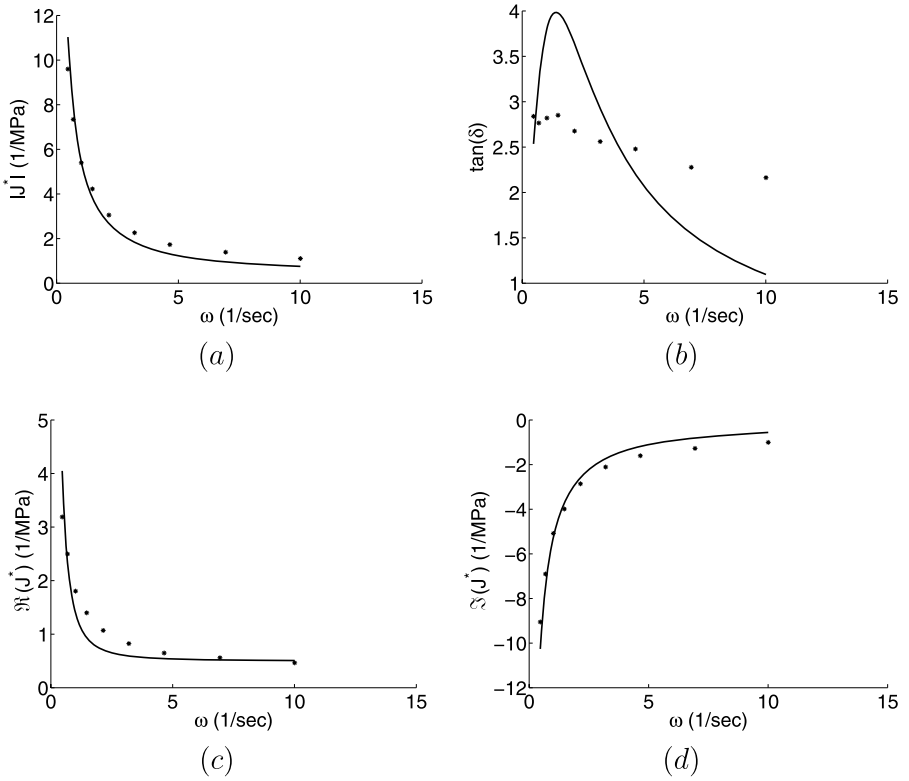

Fig. 8 This figure shows the best fit to the Cerni data by a modified Kuhn model (MKM) using the procedure described in the text. The four plots are the four representations of the complex fit used in the previous figures

the case of data with larger values of $\tan\delta$. Our fitting procedure for GKM can obviously be used also to fit an MKM model simply by imposing $\alpha = 0$ during the fitting. The results are illustrated in Figs. 7 and 8. Clearly this fit is inferior to the GKM fit and misses important features of the data.

In the MKM model, the parameter λ is quite important, whereas it is less important for GKM. Indeed, the parameters for the best GKM fits described above have values of λ close to 0. The reason for this difference in behavior between MKM and GKM is that the integral in (3) is finite when $\lambda = 0$ provided $\alpha > 0$, whereas it is infinite when $\alpha = 0$ (the MKM) and $\lambda = 0$. Thus, MKM is expected to be much more sensitive to the choice of λ than GKM.

References

Cerni, G.: Influence of the conditioning time on the rheological properties of bitumens at intermediate temperatures: loading time–temperature–conditioning time superposition principle. Road Mater. Pavement Des. **2**(4), 379–401 (2001)

Dietrich, L., Lekszycki, L., Turski, K.: Problems of identification of mechanical characteristics of viscoelastic composites. Acta Mech. **126**, 153–167 (1998)

Golden, J.M., Graham, G.A.C.: Boundary Value Problems in Linear Viscoelasticity. Springer, Berlin (1988)

Kuhn, W., Kunzle, O., Preissmann, A.: Relaxationszeitspektrum elastizitat und viskositat von kautschuk. Helv. Chim. Acta **30**, 307–328, 464–486 (1947)

Lubliner, J., Panoskaltsis, V.P.: The modified Kuhn model of linear viscoelasticity. Int. J. Solids Struct. **29**(24), 3099–3112 (1992)

Papoulia, K.D., Panoskaltsis, V.P., Korovajchuk, I., Kurup, N.V.: Rheological representation of fractional derivative models in linear viscoelasticity. Rheol. Acta (2008, submitted)

Royden, H.L.: Real Analysis, 3rd edn. Macmillan, New York (1988)